Journal of Materials Chemistry C

Accepted Manuscript

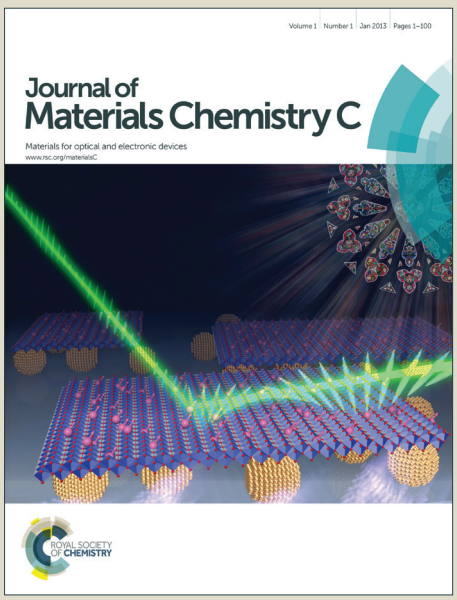

ROYAL SOCIETY OF CHEMISTRY

www.rsc.org/materialsC

Journal Name Journal of Materials Chemistry C Dynamic Article Links ►

Cite this: DOI: 10.1039/c0xx00000x

www.rsc.org/xxxxxx

ARTICLE TYPE

Long-lasting luminescent $ZnGa_2O_4:Cr^{3+}$ transparent glass-ceramics

Sébastien Chenu[*a,b], Emmanuel Véron[a], Cécile Genevois[a], Alain Garcia[b], Guy Matzen[a], Mathieu Allix[*a]

Received (in XXX, XXX) Xth XXXXXXXXX 20XX, Accepted Xth XXXXXXXXX 20XX
DOI: 10.1039/b000000x

Highly transparent $ZnGa_2O_4$ glass-ceramic materials are elaborated via a simple heat treatment of a $55SiO_2$ - $5Na_2O$ - $17ZnO$ - $23Ga_2O_3$ parent glass composition which presents nanoscale spinodal phase separation. This optimized glass-ceramic exhibits 50 wt% of $ZnGa_2O_4$ nanocrystals showing an homogeneous and tuneable size. To describe the crystallization process, the glass and glass-ceramic nanostructures are studied by high resolution scanning transmission electron microscopy analysis coupled to *in situ* high temperature X-ray diffraction and optical measurements. From these results, an original mechanism is proposed to explain the crystallization process occurring in a spinodal phase separated glass. Remarkably, red long-lasting luminescence arising from the whole sample volume is observed in the Cr^{3+} doped transparent glass-ceramics, opening the route to a wider range of performing applications for this famous zinc gallate persistent phosphor.

INTRODUCTION

A long-lasting luminescent material presents light emission during a long time (i.e. minutes or hours) after stopping the excitation source.[1] Such phosphors have been of great research interest as night or dark environment vision materials for a wide range of applications such as security signs, emergency route signage, identification markers, or medical diagnostics.[2] Among the eligible materials, the red long-lasting luminescence properties of the $ZnGa_2O_4:Cr^{3+}$ spinel material have been extensively studied, especially for application in *in vivo* bio-imaging.[3-5] Different attempts have been carried out to improve the emission intensity and duration[3, 6] and the long lasting luminescence mechanism has been revealed.[7] Recently, $Zn_{1+x}Ga_{2-2x}(Ge/Sn)_xO_4$ ($0 \le x \le 0.5$) spinel solid solutions have been reported[8] to exhibit very bright and long lasting red luminescence during more than 360h.[9, 10] In these studies, the persistent phosphors are elaborated by a usual solid-state process which yields opaque polycrystalline ceramic materials. Therefore, only the surface of the material is active for light emission, thus limiting the field of applications such as signage to luminescent paints or inks.[9, 10]

Combining the ability to transmit light in all the material volume and the intrinsic advantages of a crystalline host, transparent crystallized materials have attracted much attention for optical device applications.[11] The elaboration of a transparent zinc gallate crystalline material would clearly be a breakthrough leading to strongly enhanced emission intensity and would thus drive the development of new technologically relevant applications. To elaborate such transparent ceramics, controlled crystallization from glass appears to be a method of interest. Such prepared materials exhibit various advantages such as cost-effectiveness, mass production, and easy shape control which make them alternative candidates to current single-crystal technologies.[12, 13] Recently, an innovative method has been developped to elaborate dense polycrystalline ceramics by full and congruent crystallisation from a massive glass.[14-16] However, this alternative elaboration route requires congruent crystallization from glass, i.e. vitrification of the aimed ceramic composition, which is not achievable in the case of the zinc gallate spinel composition.

Nevertheless, this challenge can be overcome via the use of glass-ceramic technology.[17] The absence of porosity, the control of the microstructure and the possibility of high transparency in glass-ceramic materials have allowed a large variety of optical materials to be designed and commercialized.[18, 19] Moreover, glass-ceramic materials are elaborated by fast and cost-efficient glass-forming process and allow sophisticated and large scale materials with higher doping concentrations to be designed. The development of transparent glass-ceramics usually consists either (i) in matching the refractive index of the crystalline phase with the one of the residual glass matrix or (ii) in controlling the size of the crystals in order to remain below a critical size (generally inferior to one fifth of the incident wavelength). The first method is particularly complex to realize so that only a few examples have been reported.[18, 20] Most commonly, a perfect control of the glass crystallization leading to nanocrystals homogeneously distributed in the glass matrix is used to achieve transparent glass-ceramics.[17, 21] According to the Rayleigh-Gans-Debye[22] or Hendy theories,[23] the size of the crystals is of primary importance to minimize light scattering. In this sense, nucleating agents favoring a strong nucleation rate, such as ZrO_2 and/or TiO_2, have been introduced and are usually coupled to a limited crystal growth step.[21, 24] The size of the crystals can equally be controlled via phase separation mechanism as demonstrated in oxyfluoride systems.[25-30]

Recently, the authors have demonstrated the possibility to control the phase separation size in germanate glasses by careful adjustment of the nominal composition. As a result, highly transparent glass-ceramics containing zinc gallogermanate spinel materials could be prepared.[31] However, these glass-ceramic materials had to be crystallized at relative low temperature to remain transparent (above ~650°C an uncontrolled crystallization of the germanate matrix was observed, leading to transparency loss). This temperature limitation prevents the synthesis of high crystallinity materials while this crystallinity appears to be a requirement to obtain long-lasting luminescence properties in $ZnGa_2O_4$.[32] Silicate glasses are known to have higher crystallization temperature than germanate matrices, which makes them potential candidates to overcome this major drawback. Transparent silicate glass-ceramics based on spinel materials have received a lot of attention[33-35] although the zinc gallate phase has never been reported in such materials. Only a nanometer scale zinc gallate spinel material has been elaborated via a sol-gel route but the proportion of the crystalline phase is low (~10%) and no long lasting luminescence can be obtained given the low crystallization temperature.[36, 37]

Here we report on transparent glass-ceramic materials containing 50 wt % of $ZnGa_2O_4$ spinel nanocrystals which are obtained by controlled crystallization of a zinc gallosilicate phase separated parent glass. Remarkably, the Cr^{3+} doped materials exhibit red long-lasting luminescence arising from the whole material volume.

EXPERIMENTAL PROCEDURE

Material synthesis: SiO_2 - ZnO - Ga_2O_3 - Na_2O glasses doped with 0.1% Cr^{3+} (Cr^{3+} was considered as a substituent to Ga^{3+}) were prepared by conventional melt-quenching technique. ZnO (Alfa Aesar, 99.99 %), Ga_2O_3 (Alfa Aesar, 99.999 %), SiO_2 (Alfa Aesar, 99.8 %), Na_2CO_3 (Fluka, ≥ 99 %) and Cr_2O_3 (Merck 99.9%) commercial starting powders were weighted in appropriate amounts, intimately mixed in an agate mortar with ethanol to ensure homogeneous repartition of Cr_2O_3 and then heated in a platinum crucible at 900°C for 6h in particular to remove CO_2. The mixture was subsequently melted at 1600°C during 30 min in an electrical muffle furnace under air atmosphere and the melt was quenched from high temperature by immersion of the bottom of the crucible in water. The glass samples were then annealed at 550°C (i.e. about 100 °C below the glass transition temperature determined from DSC measurement) during one hour to release thermal residual stress, and finally cooled down to room temperature. To obtain the final glass-ceramic materials, the glass was introduced at room temperature in an electrical furnace, heated under air atmosphere at 10°C/min up to a temperature between 900°C and 1200°C and maintained during 10 minutes, before being cooled down to room temperature at 10°C/min.

Characterization methods: Glasses were characterized by differential scanning calorimetry (DSC) measurements performed under argon atmosphere on a Setaram MULTI HTC 1600 instrument using a heating rate of 10°C/min. The glass transition and the crystallization temperatures were determined from a 100 mg bulk sample introduced in a platinum crucible.

In situ high temperature diffraction data were performed on a D8 Advance Bruker diffractometer ($CuK\alpha_{1,2}$ radiation) equipped with a Vantec-1 linear detector and a HTK1200N Anton Paar oven chamber based on a Kanthal® resistive heating attachment. The glass powder sample was placed in a corundum crucible and heated from RT to 1200°C at 10°C/min. Isotherm data were collected between 15 and 80° (2θ) with a 0.024° step size. The Rietveld method was used to quantify the amorphous phase by using an internal standard with a well-known weight percentage.[38, 39] 63.4 wt% of $55SiO_2$-$5Na_2O$-$17ZnO$-$23Ga_2O_3$ glass-ceramic sample obtained after crystallization at 1000°C for 10 min were intimately mixed in an alumina mortar with 36.6 wt% of lithium carbonate (Li_2CO_3, Aldrich purity >99.0%). The choice of this standard is based on its low absorption (about 15 cm^{-1}) and very few diffraction peaks overlapping with the $ZnGa_2O_4$ spinel structure. Considering the low X-ray micro-absorption contrast (product of linear absorption and particles sizes of all the phases in the sample) no Brindley correction[40] was applied. The X-ray powder diffraction pattern was collected from 13° to 135° in 2θ with a 0.01° step. Quantification via Rietveld refinement was performed using the JANA software[41] using a fundamental approach for the line profile.[42]

Transmission electron microscopy (TEM) was used to characterize the nanostructure of both the glass and glass-ceramic materials. TEM images were collected on a Philips CM20 transmission electron microscope. The samples were prepared by two different ways. On the one hand the samples were first crushed in ethanol, and a drop of the solution containing a small amount of material in suspension was deposited onto a carbon-coated copper grid. On the other hand the samples were previously mechanically polished with a tripod and inlaid diamond discs until 50 µm thickness. The foils were finally thinned by argon ion bombardment (PIPS).HRTEM and STEM images and elemental compositions were performed using a JEOL ARM200F (JEOL Ltd.) cold FEG operating at 200kV and S/TEM double Cs corrected. Scanning transmission electron microscopy–high angle annular dark field (STEM-HAADF) images were acquired with an 8 cm camera length and a 0.13 nm probe size. Elemental compositions were determined by STEM-EDX using a same 0.13 nm probe size.

Optical characterizations were carried out on bulk materials after cutting and mechanical polishing. The transmission measurements were collected over the 250 - 7000 nm range using a double beam commercial spectrophotometer (Cary 5000) equipped with a Photomultiplier and a PbS photocell for visible and near infrared ranges and using a FTIR spectrometer Bruker Equinox 55 for the infrared range. The transmittance measurement was confirmed using a collimated HeNe laser emitting at 632.8 nm and a powermeter placed at a distance of 15 cm from the sample. Luminescence properties were measured using a Horiba Jobin Yvon FL3 fluorimeter equipped with a xenon lamp, double monochromator and a Hamamatsu photomultiplier tube (model: R955P).

The refractive index was measured at a wavelength of 589 nm with an Atago refractometer on optically polished samples.

RESULTS AND DISCUSSION

Transparent $ZnGa_2O_4$ glass-ceramic. Transparent glass-ceramics showing exclusively $ZnGa_2O_4$ spinel nanocrystallites of 15–45 nm have been elaborated by a single and direct heat treatment at 1000°C for 10 min of the $55SiO_2$-$5Na_2O$-17ZnO-$23Ga_2O_3$ parent glass. The TEM image presented Figure 1a shows numerous, relatively monodisperse, and well separated parallelepipedic shape nanocrystals lying in a glass matrix. The embedded selected area electron diffraction (SAED) pattern clearly shows the presence of discrete diffraction rings with well-defined spots matching the $ZnGa_2O_4$ spinel structure and attesting the good crystallinity of the material.

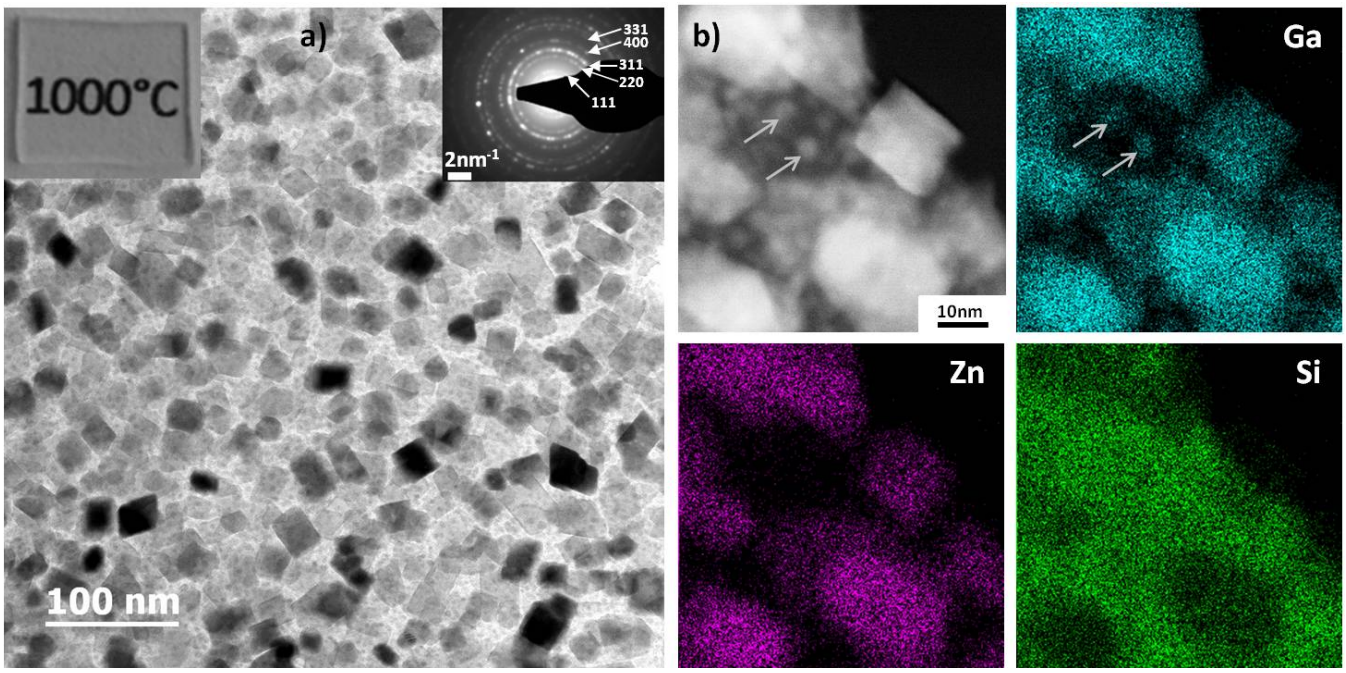

Figure 1. (a) Bright field TEM micrograph of the $55SiO_2$-$5Na_2O$-17ZnO-$23Ga_2O_3$ glass-ceramic material obtained after crystallization at 1000°C for 10 min. A photograph of the material and the corresponding selected area electron diffraction pattern are embedded. (b) STEM-HAADF image of the same $55SiO_2$-$5Na_2O$-17ZnO-$23Ga_2O_3$ glass-ceramic with associated Ga (cyan), Zn (purple) and Si (green) STEM-EDX elemental maps showing the localisation of Zn and Ga in the crystals.

The Ga, Zn and Si STEM-EDX elemental maps shown in Figure 1b reveal that Zn is fully localized in the crystals, meaning that starting from the $55SiO_2$-$5Na_2O$-17ZnO-$23Ga_2O_3$ nominal composition, 17 ZnO (and 17 Ga_2O_3) have reacted to form the $ZnGa_2O_4$ nanocrystals, leading to an impressive 50 wt% calculated crystal content. This crystallized fraction has been confirmed by quantitative Rietveld refinement (47±1 wt%, Figure S1). The matrix appears composed of almost pure SiO_2. The presence of very small amorphous Ga enriched areas within the silica matrix (pointed by grey arrows on Figure 1b) will be discussed in the crystallization mechanism section. One can note that contrary to the TEM images, STEM-high angle annular dark field (HAADF) images exhibit crystallites with a brighter contrast than the matrix. The contrast observed in these micrographs is linked to the density of the phases, thus allowing a chemical contrast to be obtained. As d = 6.2 $g.cm^{-3}$ for $ZnGa_2O_4$ and d = 2.6 $g.cm^{-3}$ for SiO_2, $ZnGa_2O_4$ consequently appears brighter than SiO_2.

Microstructure study. In order to explain the high transparency observed in these $ZnGa_2O_4$ glass-ceramic materials, the microstructure has been investigated into details. As previously stated, the transparency of glass-ceramic materials is usually correlated to the size of the crystals. Indeed, according to the Rayleigh-Gans-Debye theory[22], a sufficiently small size of crystals leads to minimization of the light scattering (crystals below ~ 70 nm are typically required for high transparency in the visible range). A perfect control of the crystallite size is thus necessary to ensure transparency.

As illustrated in Figure 2a, the $55SiO_2$-$5Na_2O$-17ZnO-$23Ga_2O_3$ glass presents a nanometer scale spinodal phase separation, i.e. a microstructure with two interpenetrated glass phases with nanometer domain sizes. It should be noted that the composition of the parent glass is adjustable to the desired microstructure as large variations of the SiO_2 and Na_2O contents are possible.[43] As previously reported by the authors in the analogous germanate system[31], the size of the phase separation can be tailored in the glass via the nominal composition. This behavior is confirmed in this silicate system where an increase of the Na_2O content leads to a decrease of the size of the phase separation whereas an increase of the SiO_2 content slowly leads to a nucleation-growth phase separation mechanism (Figure S2).

The $55SiO_2$-$5Na_2O$-17ZnO-$23Ga_2O_3$ glass ceramic samples crystallized at 900°C and 1000°C present nanometer scale crystals as shown in Figure 2b and c. Similar TEM images recorded for additional temperatures are presented in Figure S3. The crystal size distribution of these glass-ceramics determines from these images is presented in Figure 2d and clearly shows a progressive increase of the average size and of the size distribution with the temperature. The curve profiles

are relatively narrow and the maximum size remains smaller than 45 nm (28.3 nm average size with σ = 6.3) for the glass-ceramic elaborated at 1000°C. This material presents a high degree of crystallinity, with no sign of defects, as demonstrated by the HREM image presented in Figure 2e. Above 1000°C, the size distribution becomes much larger and the presence of a few crystals of nearly 100 nm large explain the beginning of transparency loss in the visible range leading to an opalescence aspect.

As suggested by the similar microstructure of the glass and the glass ceramic materials (Figure 2), the nanometer scale phase separation observed in the parent glass appears to restrain the crystal growth during the heat treatment. As the size of the phase separation can be tailored via the nominal glass composition, the control of the crystal size in the glass-ceramic material is made easier via designing the phase separation size in the parent glass. Thus, the specific spinodal phase separated microstructure allows transparent glass-ceramics to be obtained via a single heat treatment and do not require a two step crystallization process as usually considered in the common nucleation and growth crystallization process[21].

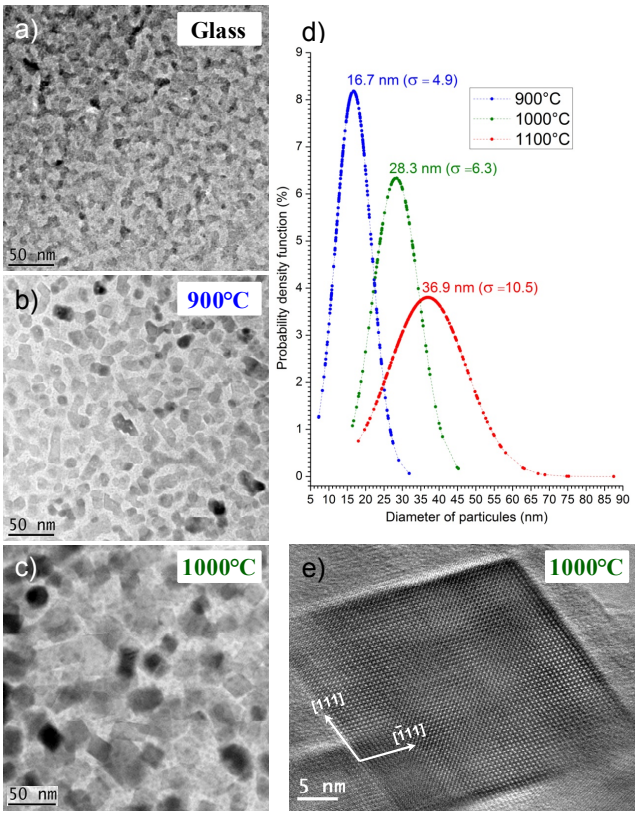

Figure 2. Bright field TEM images of the $55SiO_2$-$5Na_2O$-$17ZnO$-$23Ga_2O_3$ (a) glass and corresponding glass-ceramic materials heated at (b) 900°C and (c) 1000°C. (d) Size distribution with standard deviation (σ) of the $ZnGa_2O_4$ crystals for glass-ceramics crystallized at different temperatures (900, 1000 and 1100°C). (e) [0-11] HREM micrograph of the glass-ceramic crystallized at 1000°C.

In situ X-ray thermodiffractometry measurements presented in Figure 3a were performed on the $55SiO_2$-$5Na_2O$-$17ZnO$-$23Ga_2O_3$ glass material. While heating, several broad diffraction peaks appear from 675°C and correspond to the nanometric crystallisation of $ZnGa_2O_4$ (JCPDS 71-0643). Further temperature increase leads to continuous narrowing of these reflections, indicating constant crystal growth of the zinc gallate spinel crystals. Using the fundamental parameter approach, the crystallite size has been determined as a function of temperature, focussing on the representative 400 reflection, as shown in figure 3b (right vertical axis). The crystallite size appears quasi constant (~ 13 nm) up to 825°C, and then progressively evolves up to ~ 35 nm at 1100°C, in good agreement with the sizes observed by TEM. It should be noted that a small anisotropy is surprisingly observed on the spinel diffraction peaks below 1000°C. This behaviour may be explained by the existence of metastable or non well-crystallized intermediate phases forming during the first crystallization steps as previously observed in the MgO-Al_2O_3-SiO_2 system.[44] This point will be discussed in the crystallization mechanism section. The evolution of the crystallized fraction tracked via the evolution of the integrated area under the same 400 reflection is presented figure 3b (left vertical axis). A quick increase is observed up to 900°C, followed by a plateau, meaning that the maximum crystallized fraction was attained after this temperature and that the continuous crystallite size increase occuring at higher temperature would be explained by coalescence effects. The slight decrease commonly observed at high temperature is due to sintering (shrinkage) of the powder sample, thus leading to a slightly smaller analysed sample volume. A quantitative phase analysis has been performed from *ex situ* data recorded on the sample crystallized at 1000°C for 10 min with the addition of Li_2CO_3 as an internal standard. The results show a 47±1 wt% crystallized fraction (figure S1) close to the 50 wt% value calculated considering full reaction of ZnO (limiting precursor), as presented earlier in this paper. Using the fundamental parameter approach, an average crystallite size of 30±1 nm has been determined from this Rietveld refinement, in good agreement with the TEM measurements. From these observations, the 1000°C crystallization temperature appears to be an optimized process to combine high crystallized fraction, high transparency (controlled crystallite size) and high cristallinity degree. Remarkably, up to 1200°C $ZnGa_2O_4$ remains the unique crystalline phase present in the glass ceramic. This crystallization behavior was confirmed by DSC measurements performed on the same glass composition: a unique and strong exothermic peak around 710°C is clearly observed while Tg is estimated to 655 °C (Figure S4).

It should be noted that the glass composition with an equimolar quantity of ZnO and Ga_2O_3 (i.e. $55SiO_2$-$5Na_2O$-$20ZnO$-$20Ga_2O_3$) had first been synthetized. A similar phase separation microstructure was observed in the glass sample (Figure S5a). However, far from optimizing the overall quantity of zinc gallate spinel crystals formed in the glass, two crystalline phases, the $ZnGa_2O_4$ spinel and the Zn_2SiO_4 willemite, appeared simultaneously at 675°C, followed by the SiO_2 matrix crystallization at 1000°C (Figures S5b and S6). Although the coexistence of these phases below 900°C did not prejudice transparency within the material, opacification rapidly occurs at higher temperature, especially when the matrix starts to crystallize. As a consequence, this study is

focussing on the $55SiO_2$-$5Na_2O$-$17ZnO$-$23Ga_2O_3$ composition (determined by trail and error method) for which the Ga_2O_3 excess (17/23 ZnO/Ga_2O_3 ratio in the glass compared to the 1/1 stoechiometry in the $ZnGa_2O_4$ spinel) favours unique $ZnGa_2O_4$ crystallization and prevents SiO_2 crystallization.

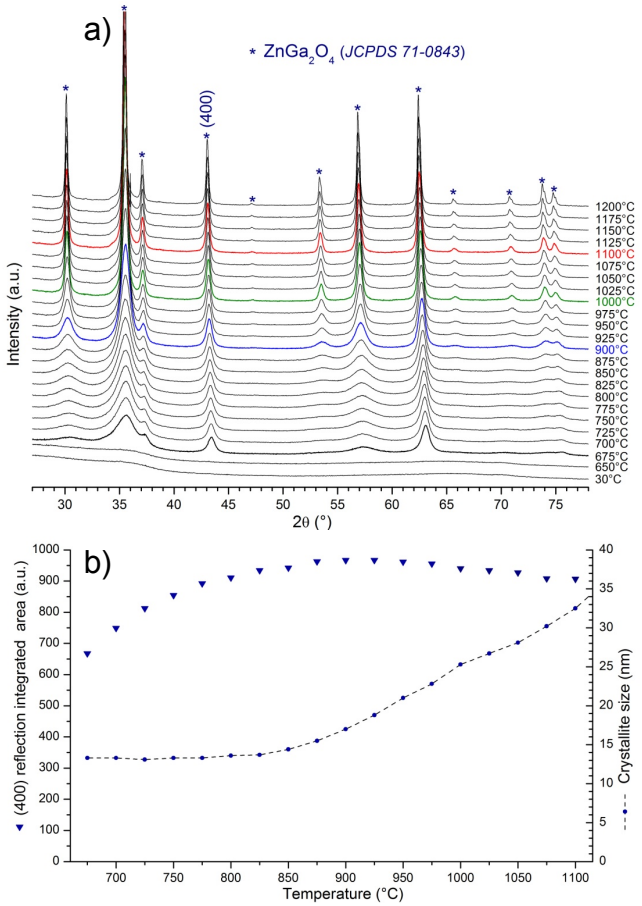

Figure 3. (a) *In situ* X-ray diffractograms collected upon heating and starting from a $55SiO_2$-$5Na_2O$-$17ZnO$-$23Ga_2O_3$ glass powder sample. The indexation corresponds to the $ZnGa_2O_4$ spinel structure (JCPDS 71-0843) appearing at 675°C. (b) Evolution of the (400) reflection integrated area (left vertical axis) and of the crystallite size (right vertical axis) versus temperature.

Crystallization mechanism. While the characteristics of the crystallization heat treatment play an important role on the crystallized fraction and especially on the crystal size, they are also governing the diffusion of the elements and thus the chemical composition of the phases formed. EDX analyses were performed on a state of the art STEM-EDX apparatus equipped with a 0.13 nm probe size. The results presented in Figures 4 and S7, along with table 1 enable to track the composition of the separated phases during crystallization. Only Si, Ga and Zn cationic elements have been quantified as the K_α(Na) edge peaks at very low energy (1.041 keV) and is strongly convoluted with the L_α(Zn) and L_α(Ga) edges (1.012 keV and 1.098 keV respectively). Moreover, Na is known to migrate under the electron beam.

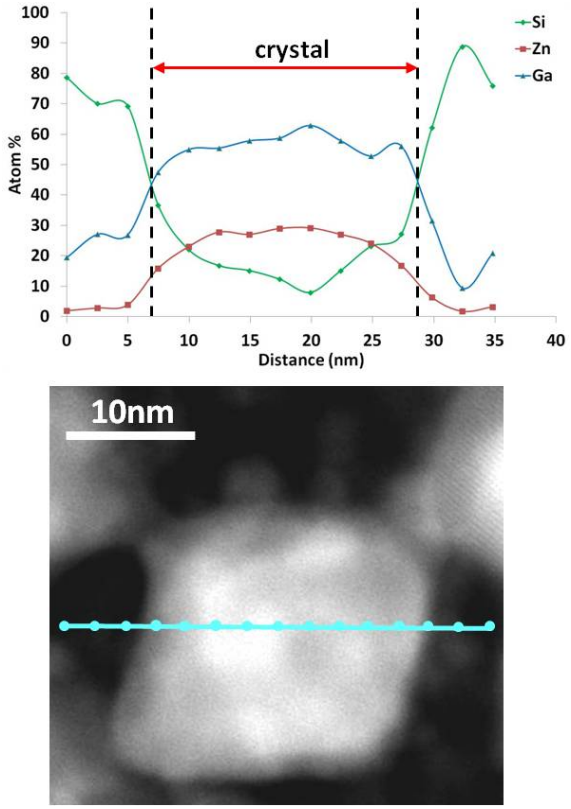

Figure 4. STEM-EDX cationic composition profile measured through a crystal of the $55SiO_2$-$5Na_2O$-$17ZnO$-$23Ga_2O_3$ glass-ceramic material elaborated at 1000°C (top). The localization of the 15 analysis points is illustrated on the associated STEM-HAADF image (down). Unfortunately the integration of a small portion of the glass matrix situated on top and/or below the crystal cannot be avoided during the EDX analysis. This leads to a smothering of the edge between the crystal and the glass matrix (this effect is more important at this edge where the crystal is thinner).

In the glass sample, a nanometer scale phase separation forming two interpenetrated glass phases is observed (Figure 2a). For clarity, the glass phase appearing bright on TEM images (i.e. dark on STEM images) will be referred to "glass matrix" as it will remain at the glassy state all along the crystallization process. By opposition, the dark phase on TEM images (bright on STEM micrographs) will be named "crystallizing phase" as it is called to transform into $ZnGa_2O_4$ crystals during the crystallization treatment. In the glass sample, the glass matrix is mainly composed of SiO_2 with a non-negligible Ga content (37 at%). In comparison, the crystallizing phase appears rich in both Ga (68 at%) and Zn (16 at%) (see elemental maps and results presented in Figure S8a and Table 1 respectively) while Si was also detected (16 at%). Special attention must be paid to the size of the crystallizing phase (around 10 - 20 nm) compared to the thickness of the sample analyzed by STEM-EDX (around 30 nm thick). Most probably, a non-negligible part of the Si content detected in the crystallizing phase may result from the glass matrix situated on top and/or below this phase. After heat treatments at 900°C and 1000°C, the Ga concentration in the crystallizing phase strongly decreases, indicating a Ga diffusion toward the glass matrix. Moreover, the Ga excess

present in the glass matrix also diffuses and leads to the formation of Ga-enriched droplets, as pointed out by gray arrows in Figure 1b. These droplets are clearly observed in the glass-ceramic elaborated at 1000°C and are already detectable in the material obtained at 900°C (Figure S8b). Their size increases with temperature, respectively from 1 - 2 nm at 900°C to 3 - 5 nm at 1000°C. Careful attention was paid not to illuminate these droplets during the glass matrix composition analyses. The results showed the remaining presence of 9 at% of Ga in the glass matrix at 1000°C, which could explain the better stability of this glass matrix versus crystallization compared to the $55SiO_2$-$5Na_2O$-$20ZnO$-$20Ga_2O_3$ nominal composition showing SiO_2 crystallization.

Concerning Zn, although its content seems to increase in the crystallizing phase versus temperature, the result is most probably biased by the departure of Ga from this crystallizing phase. This idea is confirmed by the stability of the zinc content in the glass matrix. Consequently, the diffusion of zinc appears negligible and its concentration in both phases can be considered as constant versus temperature. From this observation, discussing the Ga/Zn ratio seems more appropriate rather than focusing on the raw cationic concentrations to describe the cationic diffusion mechanisms. As a matter of fact, the Ga/Zn ratio decreases in the crystallizing phase when the annealing temperature increases (the ratio is respectively equal to 4.2, 3 and 2.1 in the glass, 900°C, and 1000°C heat treated samples) (Table 1). The latter 2.1 value is very close to the theoretical ratio of the $ZnGa_2O_4$ spinel crystal (i.e. Ga/Zn=2), proving the stabilization of the spinel structure, i.e. the end of the crystallization mechanism after the existence of metastable or non well crystallized intermediate phases with higher Ga/Zn ratio. In parallel, the Si/Zn ratio decreases upon heating in the crystallizing phase, traducing Si diffusion toward the glass matrix. This glass matrix may act as a diffusion brake given its high proportion of Si. Therefore its high viscosity is slowing down further crystal growth. As discussed previously, the Si concentration found in the crystallizing phase at 1000°C (16 at %), is in fact most probably due to the presence of the glass matrix rich in Si above and below the crystal.

Table 1. Cationic compositions (at %) of the $55SiO_2$-$5Na_2O$-$17ZnO$-$23Ga_2O_3$ glass and glass-ceramic materials obtained from EDX analyses.

Zone	Sample name	Ga	Si	Zn	Ga/Zn	Si/Zn
Glass matrix	glass	37	60	3		
	900°C	11	86	3		
	1000°C	9	88	3		
Crystallizing phase	glass	68	16	16	4.2	1
	900°C	63	16	21	3.0	0.8
	1000°C	57	16	27	2.1	0.6

A scheme summarizing the crystallization mechanisms occurring in this phase separated silicate glass and the associated cationic diffusion is proposed in Figure 5. To summarize, the crystallizing phase initially rich in Ga and Zn releases Ga and Si during spinel crystallization in order to reach the $ZnGa_2O_4$ composition (Ga/Zn = 2). As a consequence, the glass matrix is enriched in Si while the Ga excess leads to the formation of glassy Ga-Si droplets. At high temperature, coalescence of the crystals occurs, leading to transparency loss when the crystals reach a critical size (~>70 nm for the largest ones).

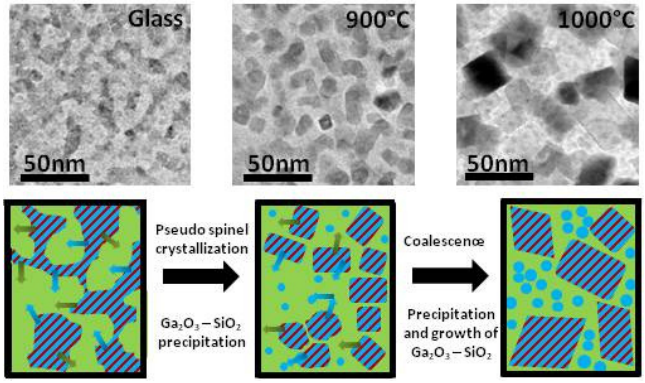

Figure. 5. Scheme of the $ZnGa_2O_4$ nano-crystallization mechanisms in a phase-separated silicate glass during heat treatment (the green area represents the glassy matrix and the blue/red striped area the crystallizing phase). Colored arrows are representing diffusion mechanisms (green for Si and blue for Ga). The experimental TEM images corresponding to each scheme are presented above.

Optical properties. Given the nanometer scale of the $ZnGa_2O_4$ crystals, the $55SiO_2$-$5Na_2O$-$17ZnO$-$23Ga_2O_3$ glass-ceramic materials exhibit high transparency with transmittance values very close to the parent glass (Figure 6).

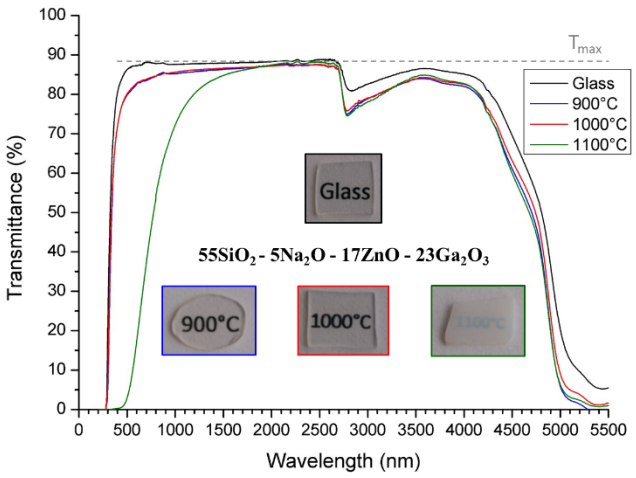

Figure 6. Transmission spectra measured through 1.5 mm thick samples of $55SiO_2$-$5Na_2O$-$17ZnO$-$23Ga_2O_3$ glass (black) and glass-ceramics elaborated at 900°C (blue), 1000°C (red) and 1100°C (green). The dashed line corresponds to the theoretical maximum transmission calculated as 88% for an average refractive index of 1.66. The photographs of the different materials are embedded.

The transmittance values obtained for the glass and spinel glass-ceramic materials elaborated up to 1000°C are very close to the theoretical maximum value, calculated as 88% for an average refractive index (n) of 1.66 (the theoretical

maximum transmission T_{max} of a material is given by the $T_{max}=2n/(n^2+1)$ equation). The high transmittance values remain constant from the visible range to the near infrared region (up to 4 µm). At 1100°C (green curve in Figure 6), the band gap transmission edge is shifted toward higher wavelengths in agreement with the material being translucent. This can be explained by the scattering of the shortest wavelengths of visible light due to the size of some crystals reaching up to 90 nm (Figure 2d). The broad absorption band located around 2900 nm is due to the presence of OH groups in the material.

Under a 410 nm excitation, Cr^{3+} doped glass-ceramic elaborated at 1000°C shows a red emission centered at 696nm (Figure 7 with the corresponding excitation spectrum presented in Figure S9) while no emission is observed in the corresponding glass (Figure S10). The emission spectrum appears similar to the data previously reported for $ZnGa_2O_4:Cr^{3+}$.[8, 45] The zero-phonon R line observed at 689 nm corresponds to the $^2E \rightarrow {}^4A_2$ transitions of Cr^{3+} occupying the octahedral site of an ideal spinel structure. The Stokes and Anti-Stokes' parts of the vibronic side bands of the R lines are showing up at the expected positions. The line observed at 696 nm originates from another type of Cr^{3+} environment much distorted compared to the ideal octahedral polyhedron. This band, labeled N2, corresponds to an environment distorted by an antisite defect located in the first cationic neighbors of Cr^{3+}. Remarkably, this transparent glass-ceramic material exhibits red long-lasting luminescence when the UV excitation is stopped.

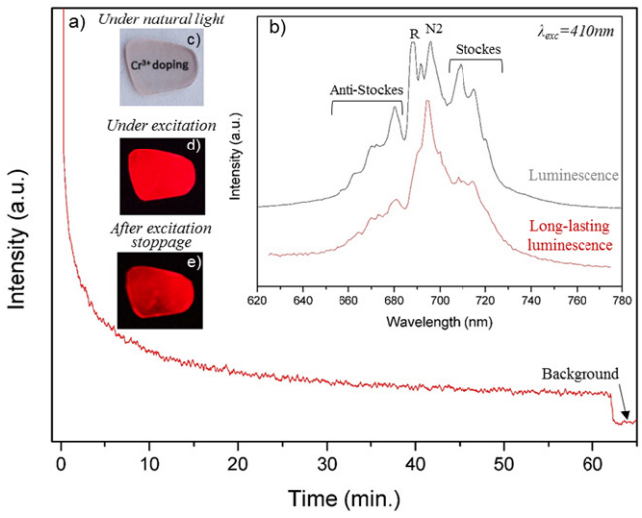

Figure 7. (a) Afterglow intensity recorded at 696 nm as a function of time for the $55SiO_2$-$5Na_2O$-$17ZnO$-$23Ga_2O_3$ 0.05% Cr^{3+} doped glass-ceramic elaborated at 1000°C. The background shows the level of the remaining afterglow signal 1h after the excitation stoppage. (b) Room temperature luminescence (black) and long-lasting luminescence (red) emission spectra obtained under a 410 nm excitation. Photographs of the glass-ceramic material have been recorded (using different time-exposure) under (c) natural light, (d) excitation (luminescence) and (e) after excitation stoppage (long-lasting luminescence). The sample is slightly thicker on the right hand side and thus evidences a volume effect of the long lasting luminescence emission.

The sample presented in Figure 7 shows a stronger afterglow emission on the right hand side of the photograph. This area corresponds to a larger thickness of the glass-ceramic, thus demonstrating the volume efficiency of the long lasting luminescence emission in these transparent glass-ceramic materials. The persistent luminescence spectrum presented below the luminescence spectrum shows a highly predominant N2 line. As N2 is a Cr^{3+} with neighboring defects, this indicates that nanoparticles crystallized from the glass possess similar type of defects as materials synthesized by solid state reaction. Moreover, this also indicates that the mechanism of long-lasting luminescence in this transparent glass ceramics is most probably the same as in solid state materials. The afterglow intensity recorded at 696 nm as a function of time reveals that this red emission is still much higher than the background an hour after excitation stoppage, attesting promising long-lasting luminescence properties.

CONCLUSIONS

Transparent silicate glass-ceramics have been elaborated by controlled crystallization of a nanometer scale phase-separated $55SiO_2$-$5Na_2O$-$17ZnO$-$23Ga_2O_3$ glass. A single appropriate heat treatment of this glass at 1000°C yields the formation of highly crystalline and transparent glass-ceramic material. A detailed crystallization mechanism has been proposed from high resolution scanning transmission electron microscopy experiments and *in situ* high temperature diffraction. The process mainly consists in gallium and silicon diffusion during the thermal treatment, enabling the formation of $ZnGa_2O_4$ nanocrystals with a narrow size distribution in a residual silicate glass phase. Remarkably, the transparent Cr^{3+} doped glass-ceramics present promising red long lasting luminescence properties arising from the whole material volume, which is a great advance in materials chemistry compared to common opaque ceramics only surface active. These materials are believed to be potential candidates to extend the actual applications of $ZnGa_2O_4:Cr^{3+}$ ceramics, especially in night environment vision materials or security signage.

Notes and references

[a] *CNRS, CEMHTI UPR3079, Univ. Orléans, F-45071 Orléans, France* *Fax: +33238638103; Tel: +33238255526; E-mail: mathieu.allix@cnrs-orleans.fr, sebastien.chenu@unilim.fr*
[b] *Institut de Chimie de la Matière Condensée de Bordeaux, 87 Avenue du Docteur Schweitzer, 33608 Pessac, France.*

† Electronic Supplementary Information (ESI) available: [details of any supplementary information available should be included here]. See DOI: 10.1039/b000000x/

Funding Sources

This work has been funding by the French ANR via the project "CrystOG" ANR-12-JS08-0002-01.

Acknowledgments

The authors acknowledge the French CNRS (FR3507) CEA METSA network and more particularly P. Ruterana (CIMAP, Caen, France), D. Pelloquin (CRISMAT, Caen, France) and the

CRMD laboratory (Orléans, France) for TEM access. P. Deniard (IMN, Nantes) is thanked for fruitful discussion on possible crystal structures.

References

1. W. M. Yen, S. Shionoya and H. Yamamoto, *Practical Applications of Phosphors*, CRC Press, Boca Raton, FL, 2006.
2. W. M. Yen, S. Shionoya and H. Yamamoto, Phosphor handbook.
3. A. Bessiere, S. Jacquart, K. Priolkar, A. Lecointre, B. Viana and D. Gourier, *Opt. Express*, 2011, **19**, 10131-10137.
4. A. Abdukayum, J.-T. Chen, Q. Zhao and X.-P. Yan, *Journal of the American Chemical Society*, 2013, **135**, 14125-14133.
5. T. Maldiney, A. Bessière, J. Seguin, E. Teston, S. K. Sharma, B. Viana, A. J. J. Bos, P. Dorenbos, M. Bessodes, D. Gourier, D. Scherman and C. Richard, *Nat Mater*, 2014, **13**, 418-426.
6. K.-H. Park, H. L. Park and S.-I. Mho, *Journal of Luminescence*, 2001, **93**, 205-212.
7. A. Bessiere, S. K. Sharma, N. Basavaraju, K. R. Priolkar, L. Binet, B. Viana, A. J. J. Bos, T. Maldiney, C. Richard, D. Scherman and D. Gourier, *Chemistry of Materials*, 2014, **26**, 1365-1373.
8. M. Allix, S. Chenu, E. Véron, T. Poumeyrol, E. A. Kouadri-Boudjelthia, S. Alahraché, F. Porcher, D. Massiot and F. Fayon, *Chemistry of Materials*, 2013, **25**, 1600-1606.
9. Z. W. Pan, Y. Y. Lu and F. Liu, *Nat. Mater.*, 2012, **11**, 58-63.
10. Z. W. Pan and Y.-Y. T. Lu, 2011.
11. A. R. Boccaccini and D. D. Silva, *Recent Patents on Materials Science*, 2008, **1**, 56-73.
12. R. Won, *Nat Photon*, 2008, **2**, 216-217.
13. S. Chen and Y. Wu, *American Ceramic Society Bulletin*, 2013, **92**, 32-37.
14. M. Allix, S. Alahrache, F. Fayon, M. Suchomel, F. Porcher, T. Cardinal and G. Matzen, *Advanced Materials*, 2012, **24**, 5570-5575.
15. S. Alahraché, K. Al Saghir, S. Chenu, E. Véron, D. De Sousa Meneses, A. I. Becerro, M. Ocaña Jurado, F. Moretti, G. Patton, C. Dujardin, F. Cussó, J.-P. Guin, M. Nivard, J.-C. Sangleboeuf, G. Matzen and M. Allix, *Chemistry of Materials*, 2013, **25**, 4017-4024.
16. K. Al Saghir, S. Chenu, E. Veron, F. Fayon, M. Suchomel, C. Genevois, F. Porcher, G. Matzen, D. Massiot and M. Allix, *Submitted*.
17. W. Höland and G. H. Beall, in *Glass-Ceramic Technology*, John Wiley & Sons, Inc., 2012, pp. 378-406.
18. G. H. Beall and D. A. Duke, *Journal of Materials Science*, 1969, **4**, 340-352.
19. I. Alekseeva, O. Dymshits, M. Tsenter, A. Zhilin, V. Golubkov, I. Denisov, N. Skoptsov, A. Malyarevich and K. Yumashev, *Journal of Non-Crystalline Solids*, 2010, **356**, 3042-3058.
20. T. Berthier, V. M. Fokin and E. D. Zanotto, *Journal of Non-Crystalline Solids*, 2008, **354**, 1721-1730.
21. G. H. Beall and L. R. Pinckney, *Journal of the American Ceramic Society*, 1999, **82**, 5-16.
22. R. Apetz and M. P. B. van Bruggen, *Journal of the American Ceramic Society*, 2003, **86**, 480-486.
23. S. Hendy, *Applied Physics Letters*, 2002, **81**, 1171-1173.
24. S. Bhattacharyya, T. Höche, J. R. Jinschek, I. Avramov, R. Wurth, M. Müller and C. Rüssel, *Cryst. Growth Des.*, 2009, **10**, 379-385.
25. C. Bocker, C. Rüssel and I. Avramov, *International Journal of Applied Glass Science*, 2013, **4**, 174-181.
26. A. De Pablos-Martín, A. Durán and J. Pascual, *International Materials Reviews*, 2012, **57**, 165-186.
27. G. Dantelle, M. Mortier, D. Vivien and G. Patriarche, *Chemistry of Materials*, 2005, **17**, 2216-2222.
28. y. ledemi, A.-A. Trudel, V. Rivera, S. Chenu, E. Veron, L. A. O. Nunes, M. Allix and Y. Messaddeq, *Journal of Materials Chemistry C*, 2014.
29. H. Lin, R. Zhang, D. Chen, Y. Yu, A. Yang and Y. Wang, *Journal of Materials Chemistry C*, 2013, **1**, 1804-1811.
30. F. Liu, E. Ma, D. Q. Chen, Y. L. Yu and Y. S. Wang, *J. Phys. Chem. B*, 2006, **110**, 20843-20846.
31. S. Chenu, E. Véron, C. Genevois, G. Matzen, T. Cardinal, A. Etienne, D. Massiot and M. Allix, *Advanced Optical Materials*, 2014, **2**, 364-372.
32. K. Uheda, T. Maruyama, H. Takizawa and T. Endo, *Journal of Alloys and Compounds*, 1997, **262**, 60-64.
33. L. R. Pinckney, B. N. Samson, G. H. Beall, J. Wang and N. F. Borrelli, in *Ceramic Nanomaterials and Nanotechnology*, eds. M. Z. Hu and M. R. DeGuire, Amer Ceramic Soc, Westerville, 2003, pp. 265-275.
34. L. Chen, C. Yu, L. Hu and W. Chen, *Solid State Sciences*, 2012, **14**, 287-290.
35. L. R. Pinckney, *Journal of Non-Crystalline Solids*, 1999, **255**, 171-177.
36. X. L. Duan, Y. C. Wu, F. P. Yu and D. R. Yuan, *Journal of Non-Crystalline Solids*, 2008, **354**, 4695-4697.
37. X. L. Duan, D. R. Yuan, X. F. Cheng, F. P. Yu, Z. Q. Liu and X. Q. Zhang, *Nanotechnology*, 2007, **18**, 175609.
38. A. G. De La Torre, S. Bruque and M. A. G. Aranda, *Journal of Applied Crystallography*, 2001, **34**, 196-202.
39. X. Orlhac, C. Fillet, P. Deniard, A. M. Dulac and R. Brec, *Journal of Applied Crystallography*, 2001, **34**, 114-118.
40. G. W. Brindley, *Philos. Mag.*, 1945, **36**, 347-349.
41. V. Petricek, M. Dusek and L. Palatinus, *Z. Kristallogr.* , 2014, **229**, 345-352.
42. R. W. Cheary, A. A. Coelho and J. P. Cline, *J. Res. Natl. Inst. Stand. Technol.*, 2004, **109**, 1-25.
43. S. Chenu, E. Véron, G. Matzen, T. Cardinal and M. Allix, 2013.
44. A. Dugué, L. Cormier, O. Dargaud, L. Galoisy and G. Calas, *Journal of the American Ceramic Society*, 2012, **95**, 3483-3489.
45. D. Gourier, A. Bessière, S. K. Sharma, L. Binet, B. Viana, N. Basavaraju and K. R. Priolkar, *Journal of Physics and Chemistry of Solids*, 2014, **75**, 826-837.

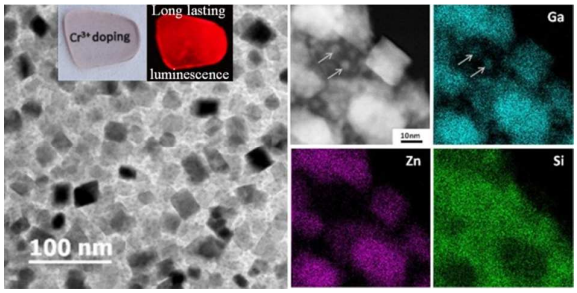

Highly transparent $ZnGa_2O_4$ glass-ceramic materials showing red long-lasting luminescence arising from the whole sample volume are reported.